Methodology for Estimating Embankment Damage Caused by Flood Overtopping

YUNG-HAI CHEN AND BRADLEY A. ANDERSON

An investigation of the erosion of highway embankments caused by flood overtopping is presented. Data collected from a series of laboratory tests and field investigations were evaluated to develop a methodology for quantitatively determining embankment damage. A computer model, verified by using laboratory and field data, was developed to simulate the hydraulics of overtopping flow and to estimate the erosion rate of the embankment. The computer model was used to generate nomographs and to develop a step-by-step procedure for estimating damage to roadway embankments. The effectiveness of five embankment protection measures was evaluated during the laboratory tests. Critical velocities and failure criteria associated with each protective measure were qualitatively established.

Estimating embankment damage caused by flood overtopping is a relatively new issue for highway engineers. Traditionally, the consequences of floods larger than the "design flood" have been ignored. Although there have been several attempts to develop an approximate method of estimating embankment damage, all attempts lacked the benefit of a set of controlled experimental data and differed by several orders of magnitude.

Numerous materials have been used for protecting embankments from flood erosion. These measures reduce embankment erosion by (*a*) protecting or strengthening the soil to increase its resistance to erosion and (*b*) increasing surface roughness to reduce the erosive force of the flood. Materials commonly used for protection include vegetation, riprap, soil cement, and geotextiles. Information about the performance of the various materials available to protect embankments from damage caused by flood overtopping is quite limited.

The objectives of this project were to review the pertinent literature, collect available field data, and conduct laboratory tests to develop a methodology to quantitatively determine embankment damage. The effectiveness and failure criteria of various types of protection were also evaluated as part of the project. The literature review, field data, and laboratory data were analyzed to develop embankment erosion equations that take into account the configuration and material characteristics of the embankment and the hydraulics of overtopping flow. A mathematical model was developed and verified using the collected field and laboratory data. The model was then used to generate design charts for estimating embankment damage caused by floods of various overtopping depths and tailwater conditions. The major results of that study are presented in this paper.

Simons, Li & Associates, Inc., 3555 Stanford Road, P.O. Box 1816, Fort Collins, Colo. 80522.

LABORATORY EMBANKMENT TEST PROGRAM

Embankment overtopping tests were conducted in an outdoor testing facility at the Engineering Research Center (ERC) of Colorado State University. The outdoor testing facility was designed to conduct tests on full-scale roadway embankments. Use of a testing facility that allows full-scale tests minimized the inaccuracies inherent in modeling the physical processes associated with the hydraulic and sediment transport mechanics of embankment erosion.

During this study soil testing was done to evaluate all fill material used in construction of the embankment test sections. Soil materials were selected in accordance with specifications provided by the FHWA and included a clayey sand mixture (Unified Soil Classification CL), as well as a sandy, more erosive soil (Unified Soil Classification SM-SC). Laboratory and field tests were performed to classify and determine the engineering properties of the fill material. The soil tests, conducted in accordance with ASTM procedures, provided information on soil classification, grain-size distribution, Atterberg limits, hydraulic conductivity, critical shear stress, shear strength, compaction characteristics, and dispersivity. Table 1 gives information on the two soils tested during this investigation.

TABLE 1 SOIL TEST RESULTS

Soil Property and Test	Unified Soil Classification	
	CL	SM-SC
Grain-size distribution		
Percent sand	40	59
Percent passing No. 200 sieve	60	41
Atterberg limits		
Liquid limit	32.7–35.1	24.4
Plastic limit	19.3–22.3	18.7
Plasticity index	11.7–15.7	5.7
AASHTO classification	A-6	A-4(0)
Compaction		
Optimum moisture content (%)	13–19	14.7
Maximum dry density (lb/ft^3)	102–111	113.5

All embankment test sections were constructed 6 ft high and allowed for a top pavement width of 12 ft and a shoulder width of 10 ft. The side slope of the embankments tested during this study varied from 2:1 (horizontal to vertical) to 3:1. The two soils described previously were used as fill material, and two roadway surfaces (soil and paved) were tested along with five embankment protection measures (grass, geoweb, enkamat,

gabion, and soil cement). The flood overtopping tests included testing a variety of side slopes, overtopping depths, water-surface drops, overtopping durations, road surfaces, and embankment protection measures. The information gained from the bare-soil tests provided a basis for judging the erosion protection afforded by pavement, vegetation, and the other embankment protection measures.

The data collected during each laboratory test included discharge, velocity, overtopping depth, water-surface profile, and embankment profile. The laboratory test data coupled with the field data collected in this study were analyzed to determine the hydraulic conditions associated with embankment overtopping flow. Given the laboratory and field data, the following analyses were specifically conducted:

- The fixed-bed embankment test data were analyzed to determine hydraulic conditions of overtopping flow including flow mode, discharge coefficients, local velocity, and shear stress immediately above the embankment surface. A mathematical model was developed to determine the hydraulic conditions of overtopping flow and was verified using the test data. The results of analysis are presented in the section entitled Hydraulics of Flow Over an Embankment.
- Data collected during the initial laboratory tests were analyzed to (*a*) determine the erosion patterns and critical shear stress of bare soil, (*b*) evaluate applicability of existing soil erosion equations, and (*c*) establish soil erosion equations that can be used to determine the rate of embankment soil erosion as a function of the soil characteristics and the hydraulics of overtopping flow. The results of analysis are presented in the section entitled Parameters and Equations Governing Erosion of Embankment.
- A mathematical model was developed by incorporating the erosion equations into the mathematical model produced for determining the hydraulic conditions of overtopping flow. This model was used to determine the embankment erosion rate due to flood overtopping. The model was calibrated using the results of tests conducted on bare soils. The effects of pavement and grass were assessed by comparing the results of tests with and without pavement and grass. The model was then applied to develop a set of nomographs for estimating embankment damage taking various flood conditions and embankment characteristics into consideration. These nomographs were verified using the field data described in the section entitled Collection of Field Embankment Damage Data. The results of the analysis are presented in Development of a Procedure for Determining Embankment Erosion Caused by Flood Overtopping.
- On the basis of the results of the laboratory tests, the effects of various protective measures on embankment stability were assessed. The critical conditions that would initiate the failure of these protective measures were determined and are discussed in the section entitled Evaluation of Embankment Protection Measures.

COLLECTION OF FIELD EMBANKMENT DAMAGE DATA

The field data collected during this project included data on roadway embankment damage caused by flood overtopping at 21 sites in 5 states. The data were collected by a joint force of personnel from the FHWA; state highway agencies; the U.S. Geological Survey; and Simons, Li & Associates, Inc. (SLA). Data were collected from five sites in Arkansas and three sites in Missouri that were affected by a flood in December 1982, four sites in Wyoming and one site in Colorado that were affected by a May 1983 flood, five sites in Arizona that were affected by a September 1983 flood, and three sites in Wyoming that were affected by a flood in August 1985. Details of field data are presented elsewhere *(1, 2)*. The field data are limited to the flow hydraulics and overtopping conditions at peak flow, total embankment damage after the flood, and minimal soil data (Unified Soil Classification and size distribution). The field data, however, proved useful for verification of the modeling assumptions and the procedure developed for determining embankment erosion.

HYDRAULICS OF FLOW OVER AN EMBANKMENT

Flow Patterns

An understanding of the hydraulics of water flowing over an embankment provides a basis for understanding the erosion process. Various flow patterns have been observed as water flows over an embankment. These flow patterns were classified by Kindsvater *(3)* as free-plunging flow, free surface flow, and submerged flow. Plunging flow occurs when the jet plunges under the tailwater surface, producing a submerged hydraulic jump on the downstream slope. Surface flow occurs when the jet separates from the roadway surface at the downstream shoulder and "rides" over the tailwater surface. Whereas free flow can be either a plunging or a surface flow, submerged flow is always a surface flow. Plunging flow generally causes more embankment erosion than does surface flow.

The free-flow transition range is the range of tailwater levels within which a given discharge can produce either a plunging flow or a surface flow, depending on the antecedent conditions. Thus, if the tailwater is initially low and the flow plunging, this pattern persists as the tailwater level rises until it reaches the upper limit of the transition range, whereupon the plunging flow changes abruptly to a surface flow. However, if the tailwater is initially high and the flow is a surface flow, this pattern persists as the tailwater drops until it reaches the lower limit of the transition range, whereupon the flow pattern changes abruptly to plunging flow. The stability or persistence of the flow patterns within the transition range is related to the inertia of the large, horizontal-axis rollers that occur on the downstream side of the embankment.

Kindsvater *(3)* presented charts for determining flow patterns over embankments. Figure 1 shows the variables used in the charts and Figure 2 shows a summary of the limits of the incipient submergence and free-flow transition ranges for a screen-wire roughness surface. Figure 2 was checked using the data collected from rigid embankment tests and evaluated to determine its applicability to large-scale embankments. The test results are also plotted in Figure 2. These results indicate that Figure 2 is applicable to the determination of the transition range between surface and plunging flow for large-scale embankments.

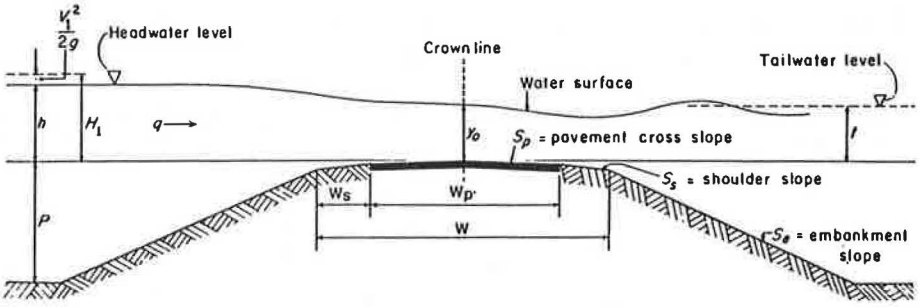

FIGURE 1 Principal variables needed to describe flow over an embankment.

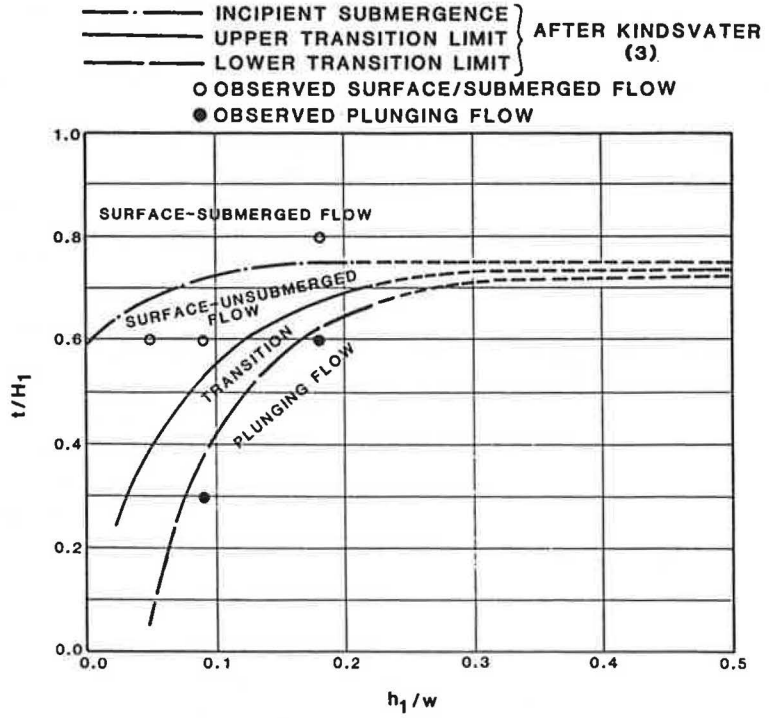

FIGURE 2 Summary of incipient submergence and free-flow transition ranges.

Examination of velocity data reveals that, for surface flow, the velocity over the downstream slope surface would be in reversed direction. Its magnitude would be relatively constant down the slope and generally less than the depth-averaged velocity. Figure 3 shows a typical water-surface and velocity profile for surface flow. Examination of the rigid embankment test data yields

$$V_r = -0.15\ V_u \tag{1}$$

Where V_r is the flow velocity over the downstream slope surface and V_u is the average velocity at the upper edge of the slope.

For plunging flow the velocity over the downstream slope surface would generally be larger than the depth-averaged velocity for the with-tailwater condition and would be the same as the depth-averaged velocity for the free-fall condition. Figure 4 shows typical water-surface and velocity profiles for plunging flow. The following relation was developed for plunging flow with the tailwater condition:

$$V_r = 0.55\ V_{uj} \tag{2}$$

where V_{uj} is the averaged flow velocity immediately upstream of a hydraulic jump.

For plunging flow with no appreciable tailwater, the representative velocity (v_r) would be the average flow velocities along the embankment

$$v_r = v_i \tag{3}$$

where v_i is the average velocity at a point (i) on the embankment.

The local shear stress can be related to local velocity by

$$\tau = {}^1/_8 f \rho\ V_r^2 \tag{4}$$

where

f = the Darcy-Weisbach coefficient,
ρ = the water density, and

V_r = a local reference velocity equal to the depth-averaged velocity over the embankment crest and upstream slope, or equal to that determined from Equation 1 or 2 for the downstream slope.

Discharge Equations for Flow Over an Embankment

The generally accepted form of the equation that computes discharge over an embankment for the free-flow condition is

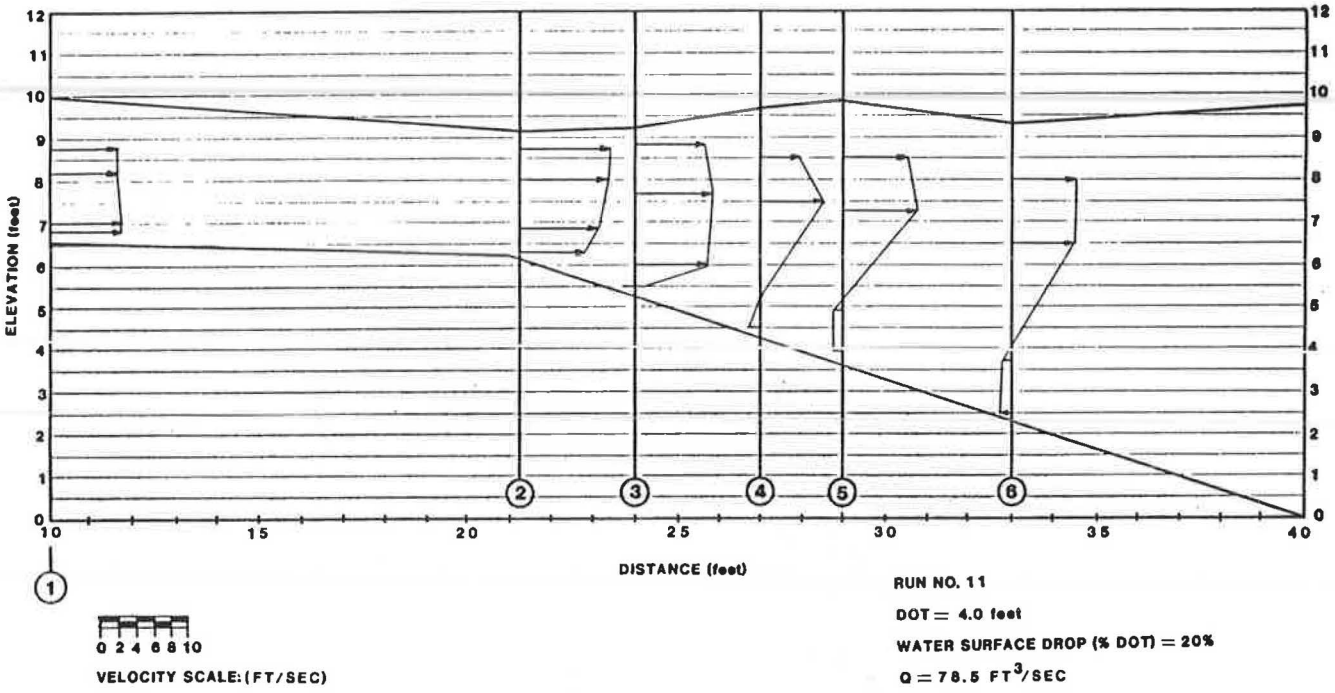

FIGURE 3 Water-surface and velocity profiles for surface flow.

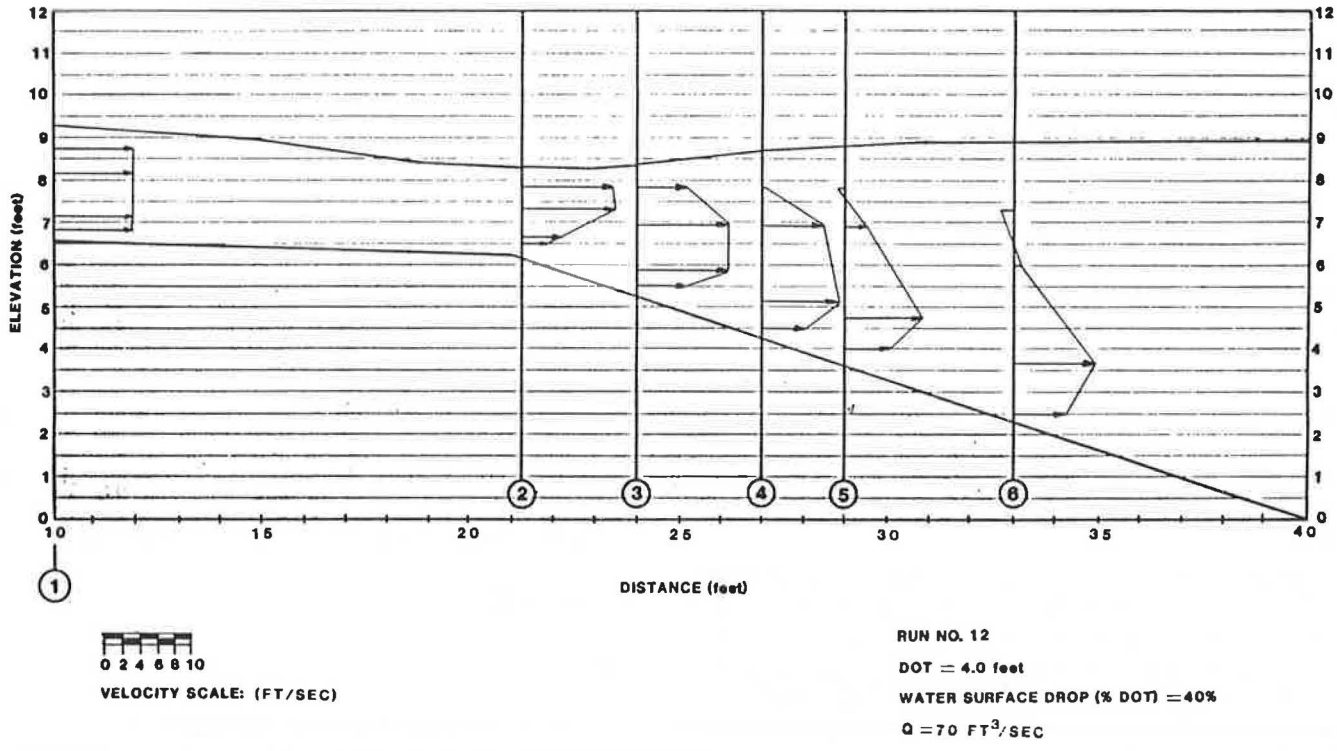

FIGURE 4 Water-surface and velocity profiles for plunging flow.

$$q = C\ H_1^{3/2} \quad (5)$$

where

q = discharge per unit width,
C = a discharge coefficient, and
H_1 = total head above the embankment crest as defined in Figure 1.

Using Kindsvater's data for a smooth roadway surface, Bradley *(4)* presented Figure 5 to determine the discharge coefficient. To determine the discharge flowing over a roadway, first enter Curve B (Figure 5) with H_1/W and obtain the free-flow coefficient of discharge (C). Should the value of H_1/W be less than 0.15, it is suggested that C be read from Curve A of the same figure. If submergence is present (i.e., if t/H_1 is greater than 0.7), enter Curve C with the proper value of submergence in percent and read off the submergence factor (C_s/C). The resulting discharge is obtained by substituting values in the expression

$$Q = C\ L\ H^{3/2}\ (C_s/C) \quad (6)$$

where

L = the length of inundated roadway,
H_1 = the total upstream head measured above the crown of the roadway, and
C and C_s = coefficients of discharge for free flow and submerged flow, respectively.

If the depth of flow varies along the roadway, it is advisable to divide the inundated portion into reaches and compute the discharge over each reach separately. The process, of course, can be reversed to aid in determining backwater for a combination of bridge and roadway configurations.

Experimental results of this study indicated that Figure 5 is applicable to the determination of the coefficient of discharge for flow over full-scale embankments. The effect of embankment side slope on the flow is insignificant except perhaps for the effect on rolling waves on the downstream side. For the free-flow case, variations in embankment height, pavement, cross slope and shoulder slope do not affect the hydraulic conditions of flow on the embankment crest.

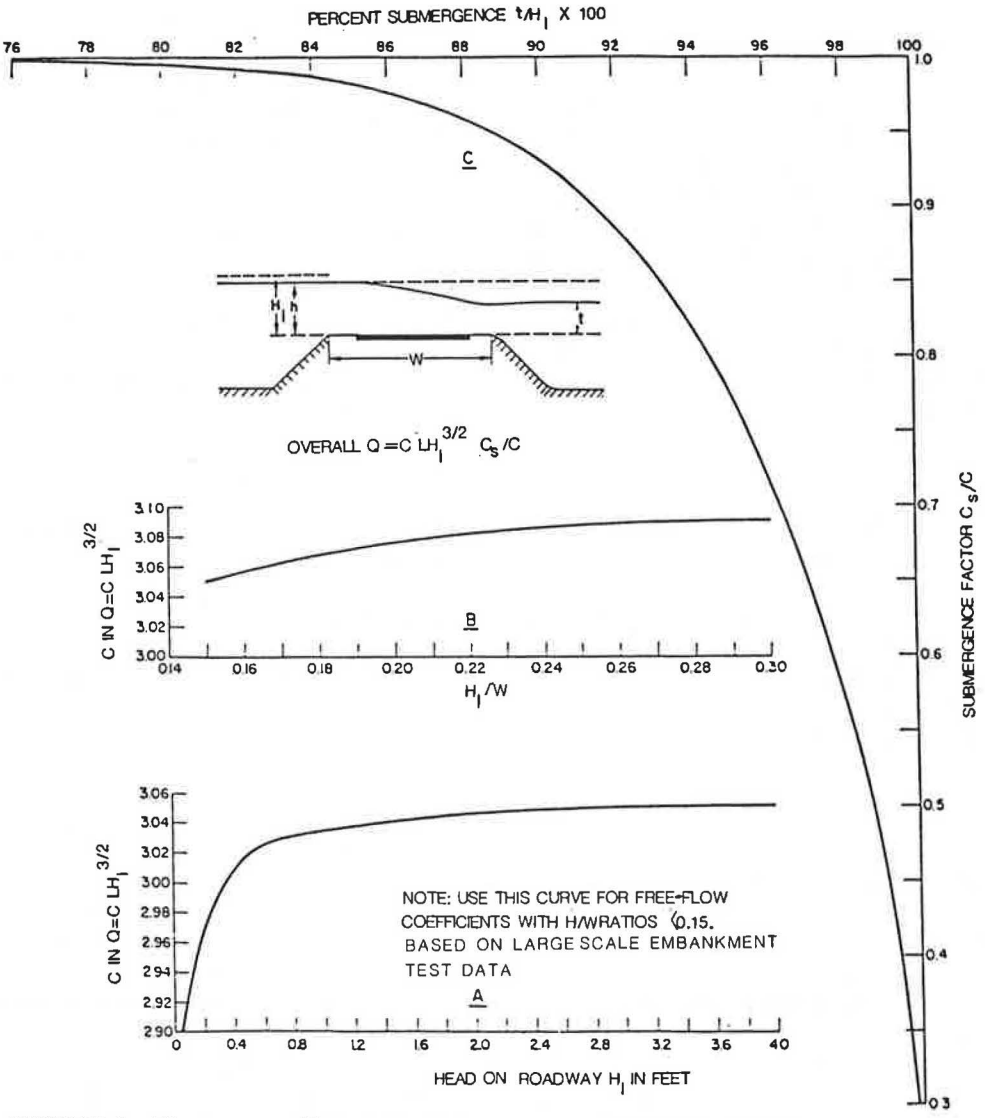

FIGURE 5 Discharge coefficients for flow over roadway embankment *(4)*.

PARAMETERS AND EQUATIONS GOVERNING EROSION OF EMBANKMENT

The erosion of soil, particularly cohesive soil, is complicated because many controlling parameters act interdependently. Principal factors involved are the physical and chemical properties of the soil itself, its behavior when partly and fully saturated, and the hydraulic properties of the flow.

When embankments are overtopped by flood waters, erosion damage can be significant because of high velocities on the downstream side of the embankment. As the shear stress exerted by the flow exceeds the critical shear stress of the soil, erosion begins. Shear stress increases with velocity. Velocity depends on the headwater and tailwater conditions. Another important parameter is the erodibility of the soil. Cohesive soil or soil with larger particles is more resistant to erosion than are noncohesive, fine-grained soils. The duration of overtopping affects the amount of damage.

The critical or permissible shear stress and velocity are defined as the largest shear stress and velocity of flow that will not cause erosion. For noncohesive materials, the following equation can be used to determine the critical shear stress *(5)*:

$$\tau_c = 0.05\ (\gamma_s - \gamma)\ d_{50} \tag{7}$$

where γ_s and γ are the unit weights of soil and water, respectively, and d_{50} is the median particle size of the soil. Equation 7 is valid for a shear Reynolds number greater than 70.

Several relations for determining critical shear stress have been developed for cohesive soil. In the study of hydraulic erosive forces required to initiate motion of cohesive soils in open channels, Smerdon and Beasley *(6, 7)* found that critical tractive force of cohesive soil correlated well with plasticity index. The relation developed for 11 uncompacted Missouri soils, ranging from a silty loam soil with little cohesion to a highly cohesive clay soil, was

$$\tau_c = 0.0034\ (PI)^{0.84} \tag{8}$$

where *PI* is the plasticity index. Because soils used in highway embankments are normally compacted, a new relationship was needed for τ_c.

Because the plasticity index is generally available or can be easily determined for different types of soils, it was decided that a power relation in the form of Equation 8 would be used in this study to determine critical shear stress. By using the data from McWhorter et al. *(8)* and soil data from this study, the following relation was obtained:

$$\tau_c = 0.019\ (PI)^{0.58} \tag{9}$$

McWhorter et al. *(8)* conducted a comprehensive study for the design of open channels using artificial lining materials. In the course of experimentation, 11 soils ranging from a noncohesive sand gravel to an inorganic clay were tested. McWhorter et al. conducted a series of tests to determine erosion rates of these soils by flow. In this study, the erosion rates were plotted versus shear stress for different soils. Regression lines were fit to the data points and then extended to zero erosion to determine the critical shear stress. These data are plotted in Figure 6 and fitted by a power function (Equation 9). The critical shear stress for the clayey sandy soil used in this project is also plotted in Figure 6. Equation 9 generally agrees with the values recommended by Chow *(9)*. However, it calculates higher critical shear stress than does Equation 8. The reason could be that Equation 9 was derived from tests of well-compacted soils (dry density ranging from about 90 to 105 lb/ft^3) and Equation 8 was derived from uncompacted soil tests (dry density ranging from about 60 to 75 lb/ft^3). Compaction increases the resistance of soil to erosion.

A number of erosion equations (*10–12* and Wiggert and Contractor and Cristofano, unpublished data) were developed for estimating embankment erosion. These equations were derived mainly from empirical approximations and limited laboratory and field data. After evaluation of existing erosion equations and the literature review, it was determined that a promising equation for estimating the embankment erosion rate is

$$E = K\ (\tau - \tau_c)^a \tag{10}$$

where

E = the detachment rate per unit area,
τ = the local effective shear stress based on hydraulic conditions,
τ_c = the critical shear stress of soil, and
K and a = empirical coefficients dependent on soil properties.

Three erosion equations were developed for the two types of soil tested in this study and the noncohesive soil tested by McWhorter et al. *(8)*. On the basis of a regression analysis of laboratory data, the following equations were developed:

1. For embankments made from highly cohesive soil such as clay (PI $\geq$ 10)

$$E = 0.000086\ (\tau - \tau_c)^{0.91} \tag{11}$$

2. For embankments made from low-cohesive soil such sandy clay (PI $\leq$ 5)

$$E = 0.00022\ (\tau - \tau_c)^{0.43} \tag{12}$$

3. For embankments made from noncohesive sand or gravel soil

$$E = 0.00324\ (\tau - \tau_c)^{1.3} \tag{13}$$

where E is the erosion rate in cubic feet per second-foot. Figure 7 shows the fitting of the experimental data.

Equations 11–13 were used to generate nomographs for estimating embankment damage caused by flood overtopping as discussed in Development of a Procedure for Determining Embankment Erosion Caused by Flood Overtopping. The experiments for evaluating effects of grass covers on embankment erosion were inconclusive. All of the tests were conducted under free-fall conditions. In tests with low overtopping depths (0.5 ft), the grass-lined embankment appeared to

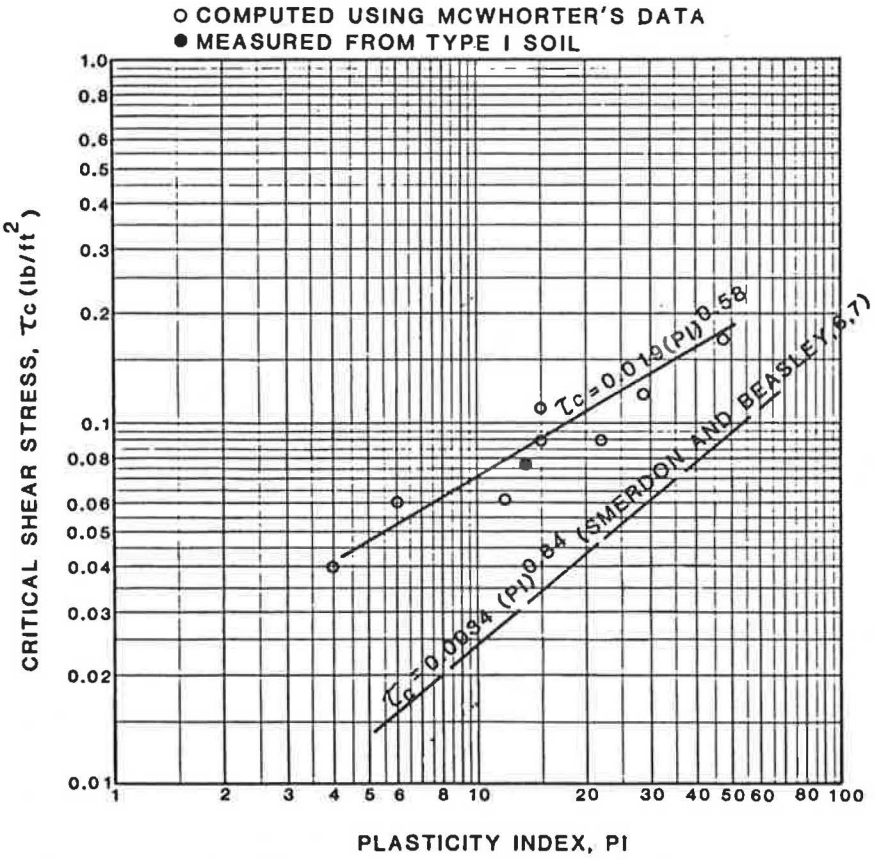

FIGURE 6 Relation of critical shear stress to plasticity index.

perform well. In tests with high overtopping depths (2 and 4 ft), clumps of grass were removed and induced the formation of local scour along the embankment. The nature of the grass cover (clumps versus uniform cover) could induce local scour and increase the shear stress near the clump of grass. A further explanation of this phenomenon could be the existence of weak spots along the embankment or areas in which the root system of the grass was not fully established. Severe toe erosion also occurred. It appeared that these areas of increased erosion, local scour, and toe erosion were related to the erodibility of the underlying soil. Therefore it is reasonable to assume that the erosion equation coefficients K and a for grass cover would be the same as those for the underlying soil and only the τ_c-value would change.

DEVELOPMENT OF A PROCEDURE FOR DETERMINING EMBANKMENT EROSION CAUSED BY FLOOD OVERTOPPING

Development of a Computer Model for Determining Embankment Erosion

A computer model was developed to determine the hydraulic conditions and embankment erosion associated with flood overtopping. Figure 8 is a flowchart of this model. Some of the steps are self-explanatory. Steps 1, 2, 13, and 14 are explained in more detail in the following list.

- Step 1: Divide the modeled embankment into computational sections. The geometry is then input as (x,z) pairs. Manning's n is input for each computational section. Chen and Cotton *(13)* presented values of Manning's n for various surfaces including rigid, soil, rock, grass, and some flexible linings.
- Step 2: Input embankment soil and structure characteristics and erosion equations. A roadway embankment can be considered to contain four layers: pavement, gravel base, grass cover, and base soil. The critical shear stresses and Manning's n-values for the four layers are input as data to the model. Also, the thicknesses of the layers in each computational section are input as data. The developed model can also consider gravel or earth embankments with or without grass and with a homogeneous or nonhomogeneous soil base. When one layer is eroded, the critical shear stress and Manning's n for the immediately lower layer are used for next time-step computation. Equation 10 is used to compute erosion rates. Depending on the characteristics of the layers, proper values of coefficients a and K are input as data.
- Step 13: Determine the erosion rate of each computational section from Equation 10 using the critical shear stress and input coefficients of the erosion equation for the surface layer. If the surface layer was eroded within a period shorter than a computational time step, the critical shear stress of the immediately lower layer would be used for the computation for the remaining time period.

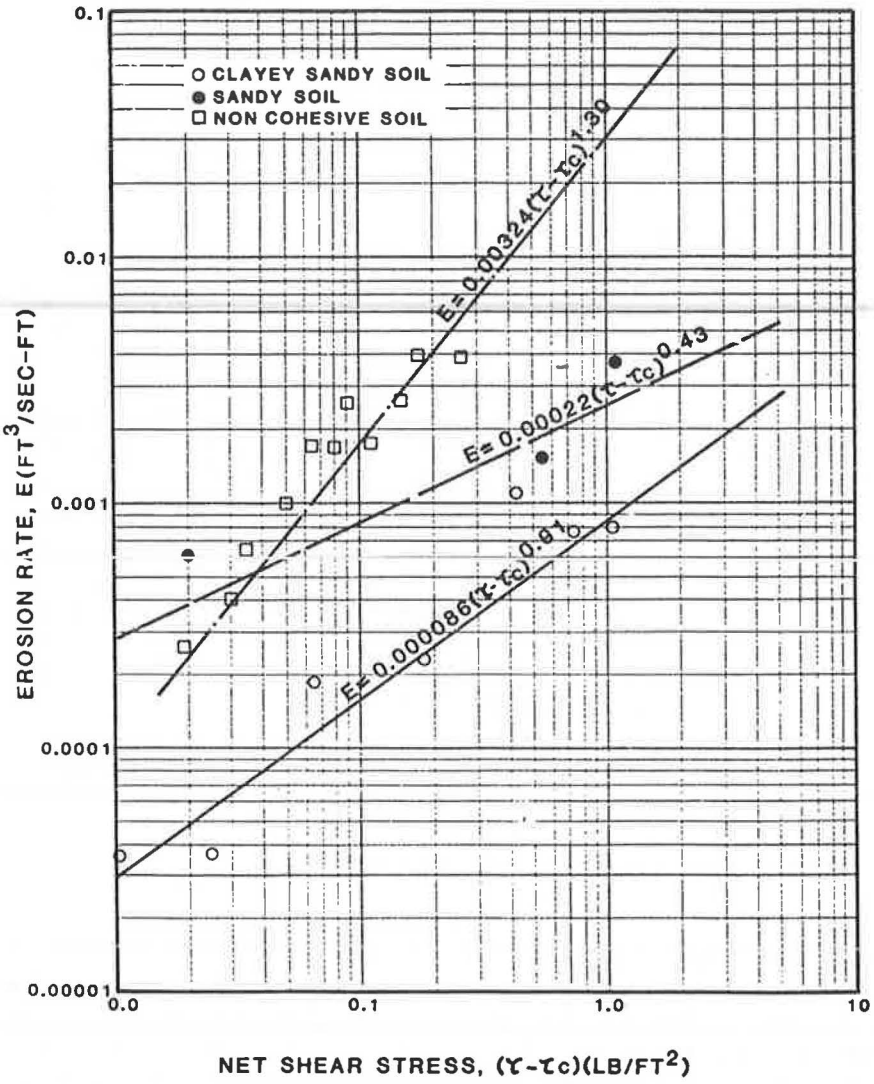

FIGURE 7 Embankment erosion equations.

• Step 14: Determine embankment bed erosion of each section during a time step. For grass, gravel, or the soil surface, the bed erosion depth is

$$\Delta Z = E\ \Delta t \tag{14}$$

where E is the erosion rate from Equation 10 and Δt is the time-step duration. For paved sections, it was assumed that damage to the pavement is not due to direct flow erosion but instead to erosion undermining the roadway base and cantilevering the pavement. Given the condition shown in Figure 9, the maximum normal stress on the pavement due to flow is

$$(\sigma_x)_{max} = M/S_m \tag{15}$$

where M is the bending movement induced by the weight of the pavement and water above a given point and S_m is the section modulus. Let D equal the average depth of flow at the middle of the undermined pavement, t the thickness of the pavement, γ_w the unit weight of water, and γ_a the unit weight of pavement. Then

$$M = (\gamma_w D + \gamma_a t)\ x^2/2 \tag{16}$$

and

$$S_m = t^2/6 \tag{17}$$

Substituting Equations 16 and 17 in Equation 15 yields

$$(\sigma_x)_{max} = [3(\gamma_w\ D + \gamma_a t)\ x^2]/t^2 \tag{18}$$

For the computer model, the undermining length (x) is assumed to be one-tenth of the eroded depth at the edge of the pavement; D is the computed flow depth at the edge of pavement; and γ_w, γ_a, and t are known variables. By substituting these values into Equation 18, $(\sigma_x)_{max}$ is computed. If $(\sigma_x)_{max}$ is larger than the allowable tension stress of the pavement (σ_a), it is assumed that the pavement from the downstream edge to its immediately upstream computational section is eroded within one time step. Then this computation section becomes the downstream edge of the pavement for the next computational step.

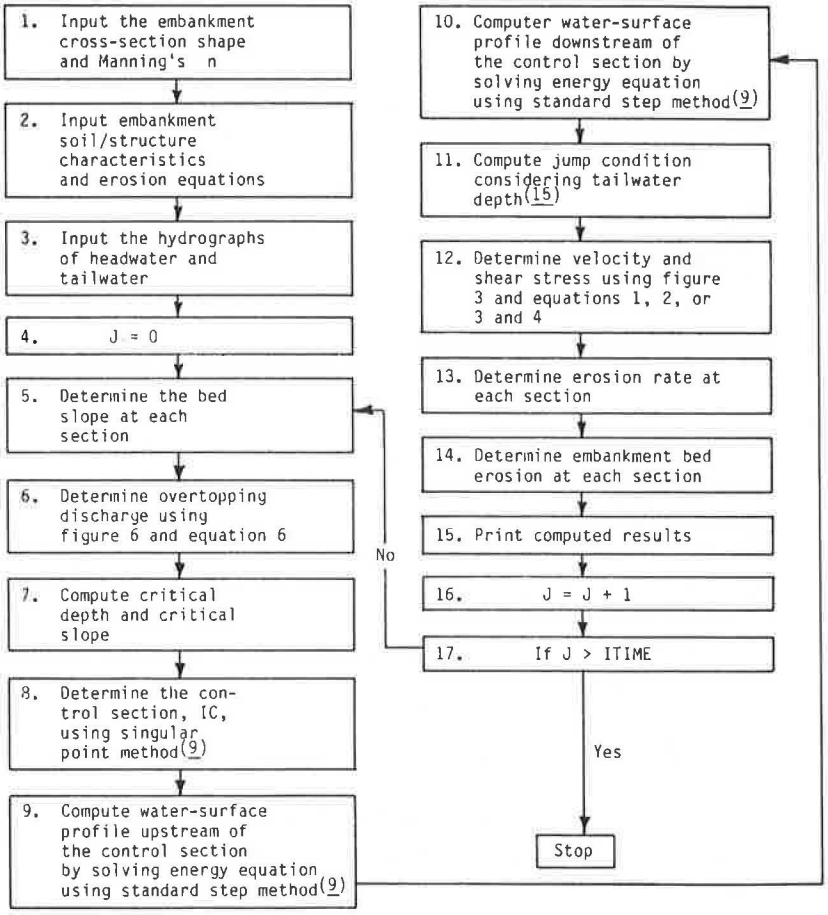

FIGURE 8 Flowchart of the computer model EMBANK.

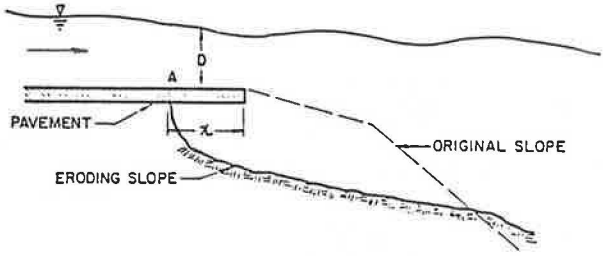

FIGURE 9 Undermining of embankment pavement.

Calibration of the Computer Model

The bare-soil embankment test data from the initial laboratory tests were used to calibrate the computer model. The geometry and soil characteristics of these embankments and overtopping headwater and tailwater depths were input to the computer program to calculate the volume of material eroded during the first hour. Then the calculated values were compared with the measured volumes during the first hour of the tests and plotted in Figure 10. The agreement is acceptable. The model was then used to develop nomographs for estimating embankment damage under various flow and embankment conditions.

Development of Nomographs for Determining Embankment Erosion Caused by Flood Overtopping

The calibrated computer model was applied to develop nomographs for estimating erosion of bare-soil and pavement embankments with and without vegetal cover under the following conditions:

- Base soils consisting of high-cohesive material, low-cohesive material, and noncohesive material;
- Paved embankment with and without Class A, C, and E grass covers;
- Embankment heights ranging from 2.5 to 15 ft;
- Overtopping depths ranging from 1 to 10 ft; and
- Ratio of tailwater depth to overtopping depth ranging from free fall to 0.9.

The computed erosion rates (averaged over a 4-hr period) were plotted in Figure 11 for 5-ft high-cohesive (PI = 13) and low-cohesive (PI = 5) bare-soil embankments and in Figure 12 for 5-ft noncohesive soil embankments ($d_{50} \cong 4$ mm). These two figures can be used to estimate erosion rates of 5-ft bare-soil embankments. Because critical shear stress is not a particularly sensitive parameter, it is suggested that Figure 11 be applied to high-cohesive soil embankments with PI $\geq$ 10 and to low-cohesive soil embankments with PI $\leq$ 5. Figure 12 should be applied to noncohesive soil embankments with $d_{50} < 8$ mm. For embankment soils with PI between 5 and 10, the erosion rate can be determined by interpolation.

Other factors considered in the procedure include the effects of pavement and grass, the duration of overtopping, and the height of the embankment. Under high tailwater conditions, most erosion of the bare-soil embankment occurred along the top and downstream shoulder. Addition of a paved surface

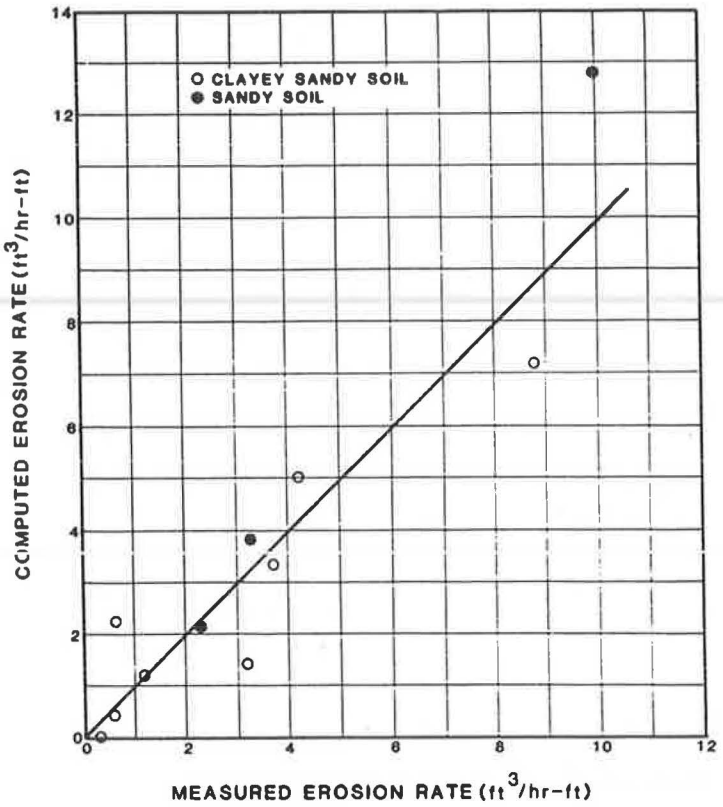

FIGURE 10 Computed versus measured erosion rate.

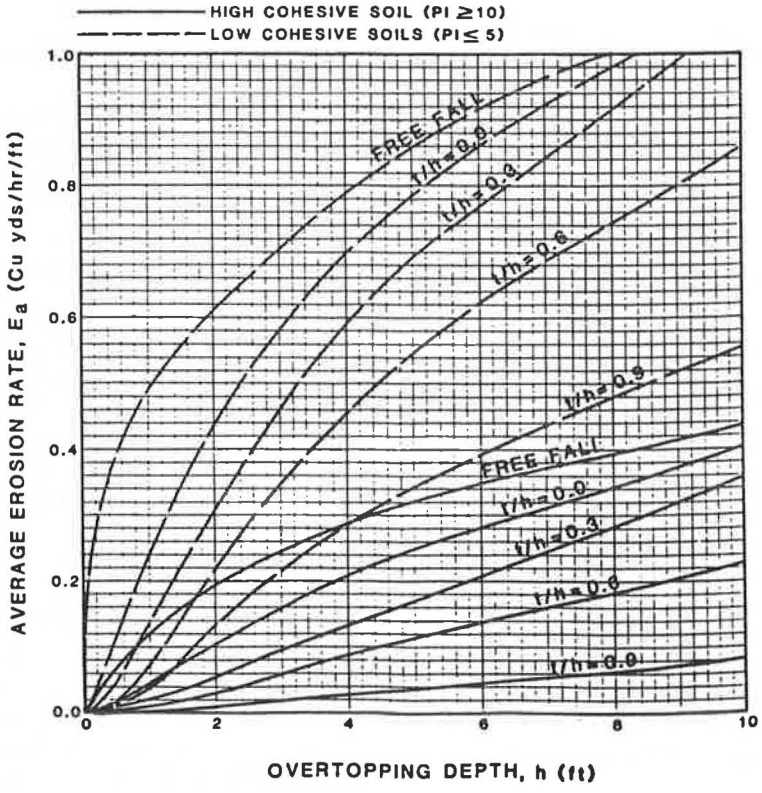

FIGURE 11 Average erosion rate during 4-hr overtopping of 5-ft cohesive bare-soil embankment.

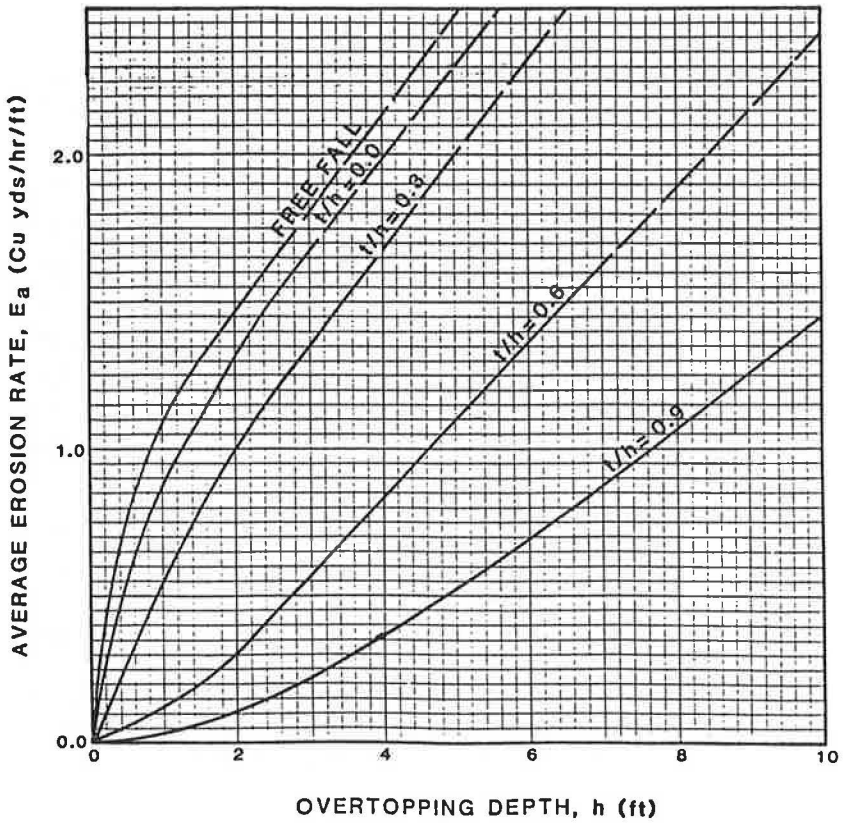

FIGURE 12 Average erosion rate during 4-hr overtopping of 5-ft noncohesive bare-soil embankment.

reduced the eroded area. The tests conducted in the study showed that erosion was reduced by as much as 50 percent with high tailwater. When tailwater was low, most erosion occurred near the downstream toe of the embankment, and the effect of pavement on embankment erosion was not as significant. A number of nomographs were generated using the computer model for estimating the average erosion rate of paved 5-ft-high embankments with and without vegetal cover on the embankment slopes. Depending on the type of fill material and the vegetation conditions, pavement coupled with vegetation cover reduced embankment erosion from 10 to 50 percent. Figure 13 shows an example of an erosion rate of a paved embankment with grass cover. The complete set of nomographs was presented by Chen and Anderson *(14)*.

The laboratory test data clearly showed that the erosion rate reduced with time. Figure 14 shows approximated relations of $\bar{E}/E_a$ versus time, based on laboratory test data, where $\bar{E}$ is the average erosion rate over a test time period and E_a is the erosion rate during the first 4 hr. With high tailwater, the water-surface profile of overtopping flow is controlled by the tailwater and remains about the same throughout the erosion of the embankment. Therefore velocity and shear stress generally decrease during the progress of embankment erosion and thereby decrease the erosion rate. With low tailwater and free-fall conditions, the reduction in erosion rate with time is less. Figure 15 shows the adjustment factor when the embankment height varies from 5 ft. Embankment erosion increases with increases in embankment height.

Figure 11, 12, or 13, coupled with Figures 14 and 15, can be applied for estimating an embankment erosion rate using the following procedure:

1. Find out the type of embankment base soil (high-cohesive, low-cohesive, or noncohesive soil), embankment height, paved or nonpaved surface, and type of vegetal cover.
2. Select the headwater depth (h), tailwater depth (t), and duration (T) for a design flood.
3. Compute t/h.
4. With h and t/h enter Figure 11 (for cohesive bare soil), Figure 12 (for noncohesive bare soil), Figure 13 (for paved cohesive-soil embankment with Class A grass cover), or other nomographs (not shown in this paper for paved embankments) to determine the erosion rate (E_a) for a 5-ft embankment. A rough estimate of the effect of pavement and vegetation is a 30 percent reduction of bare-soil embankment erosion for a surface-flow condition and a 10 percent reduction for a plunging-flow condition, if the flow shear on the slope is larger than the critical shear stress of the vegetated embankment.
5. Determine adjustment factor K_1 from Figure 14 considering the design flood duration (T).
6. Determine K_2 from Figure 15 if the embankment height is different than 5 ft.
7. Compute the average erosion rate over the design flood duration:

$$\bar{E} = K_1 K_2 E_a \tag{19}$$

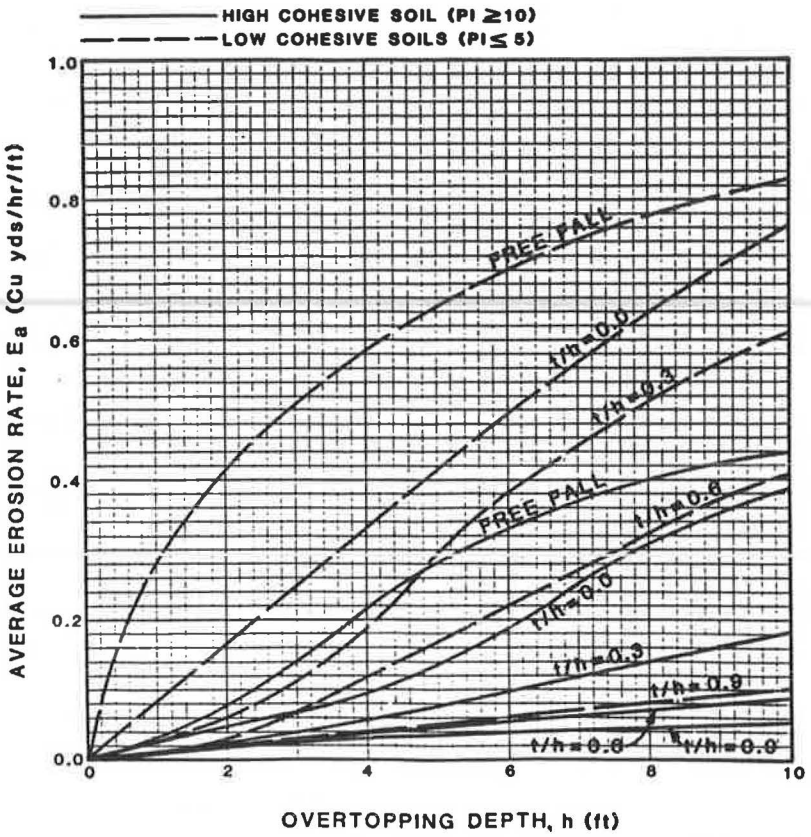

FIGURE 13 Average erosion rate during 4-hr overtopping of 5-ft paved cohesive soil embankment with Class A vegetal cover.

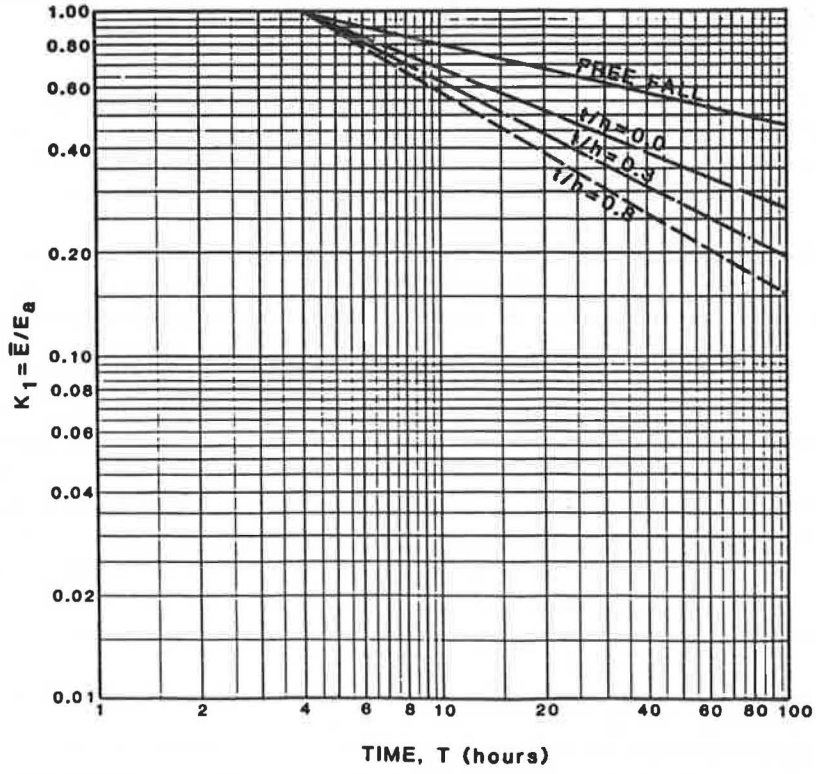

FIGURE 14 Average erosion rate change with changes in duration.

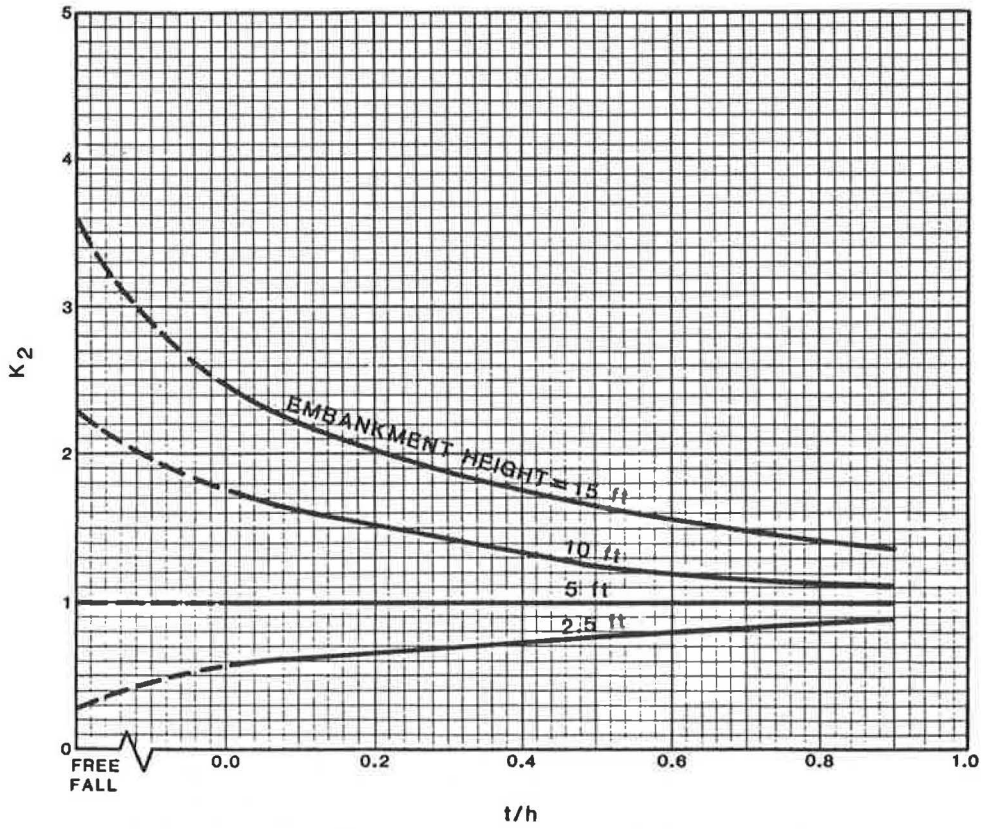

FIGURE 15 Adjustment factor taking embankment height into consideration.

8. Compute the total erosion volume:

$$V_s = ET \tag{20}$$

The procedures described were applied to the laboratory test data and the field data collected during this project. The estimated results are compared with measured erosion rates in Figure 16. The agreement is reasonably good. This indicates that the developed nomographs are useful for estimating embankment erosion rates with reasonable accuracy. However, only limited soil bases were considered in developing these nomographs, and the effects of pavement and grass were evaluated by using limited laboratory data. Therefore, for other types of embankments or for more detailed estimation of embankment erosion, the computer model developed as part of this study should be used. It is recommended that the nomographs and developed computer model be further verified or modified, or both, using additional field and laboratory data.

EVALUATION OF EMBANKMENT PROTECTION MEASURES

This study evaluated the effectiveness of several erosion protection measures, including vegetated embankments and embankments protected with gabion mattresses, soil cement, geoweb, and enkamat.

For each protective measure tested, a preliminary assessment of the failure mechanism or threshold conditions for failure of the protective measure was conducted. The failure signal was identified as a noticeable change in the water surface during the test or noticeable erosion of the protective measure or embankment material after the test.

The failure mechanism associated with the gabion mattresses appears to be related to the movement of the rocks within the mattress. The moment when the liner becomes exposed was construed as the threshold condition for failure. In general, gabion mattresses performed quite well and in no instance was the embankment in danger of erosion.

The potential failure mechanisms associated with soil cement were initially identified as the presence of surface cracks or the undermining of the layer of soil cement at the toe of the embankment. Because of the nature of the tests, neither failure mechanism was realized. A number of cycles involving freezing and thawing or wetting and drying of the soil cement layer are the catalyst needed for surface cracks to form. The relatively short testing period prevented this effect. In general, the soil cement protective measure performed quite well. After 10 hr of testing under the most severe conditions, no erosion was evident in either the soil cement or the embankment material.

For the geoweb grid confinement system, the failure mechanism appears to be associated with the boiling of rocks out of the cells of the geoweb. As the rocks are boiled out, the flow velocity directly impinges on the geoweb structure and creates an elongation of the geoweb section. The elongation effect, in turn, exposes the embankment material to direct erosion by the flowing water. In general, the geoweb performed poorly in the configuration tested by this study. Attempts were made to improve the stability of the protective measure by increasing the length and number of staples in the geoweb system. In addition, the configuration of the geoweb system was changed.

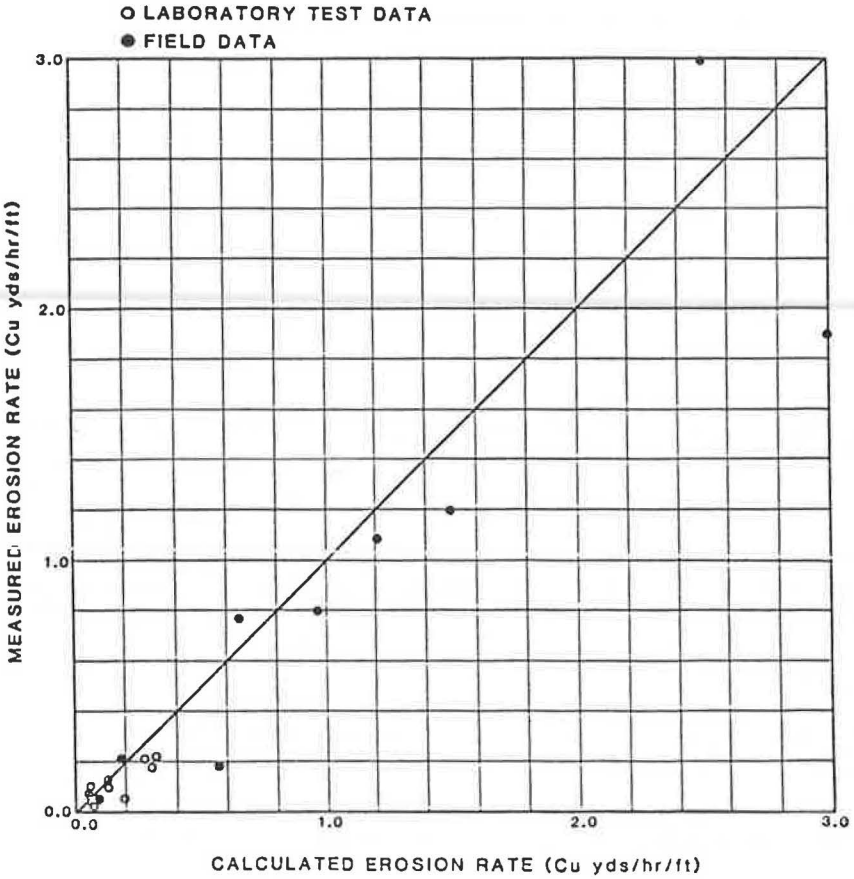

FIGURE 16 Comparison of calculated and measured embankment damage data.

The failure mechanism associated with enkamat was related to ripping or stretching of the enkamat material or noticeable erosion of the embankment beneath the enkamat. The presence of grass in the enkamat had little effect. This resulted from an unsatisfactory stand of grass (density and length) after a growth period of only 1 year. Because of the relatively short growth period, the root system was not fully developed. In all tests, erosion of the embankment material occurred as the flow velocity increased with overtopping depths greater than 1 ft. In general, enkamat afforded reasonably good erosion protection during the tests of low overtopping depths. As the overtopping depths increased beyond 1 ft, erosion of the embankment appeared to be accelerated by the presence of the enkamat.

For grass-lined embankments, the failure mechanism was associated with direct erosion or loss of grass. In tests with low velocities and overtopping depths (0.5 ft), the grass-lined embankment appeared to perform well. In tests with overtopping depths greater than 0.5 ft, pockets of grass were removed and induced local scour along the embankment. In addition to the local scour, severe toe erosion occurred during the tests involving overtopping depths of 2 and 4 ft. Although grass-lined slopes usually retard flow velocity and reduce erosion, these tests did not confirm those results.

In summary, erosion of the geoweb system started when the flow velocity exceeded 8.0 ft/sec. Rocks within each gabion were observed to migrate as the flow velocity exceeded 15 ft/sec. However, gabion still provided sufficient protection during the 15-hr testing period. Even at velocities in excess of 20 ft/sec, no failure of soil cement was observed. Damage to the enkamat material was observed when the flow velocities exceeded 10 ft/sec. The critical velocities associated with the various protective measures, as determined by the tests conducted, are given in Table 1. Table 2 gives the critical shear stress recommended by Chen and Cotton *(13)* for gabion, enkamat, and grass.

TABLE 2 CRITICAL VELOCITY ASSOCIATED WITH PROTECTIVE MEASURES

Protective Measure	Overtopping Depth (ft)	Critical Velocity (ft/sec)	Critical Shear Stress (lb/ft^2)
Geoweb	0.9	6.0	0.7
Gabion	4.0	15.0	4.0
Soil cement	4.0	>20.0	
Enkamat	2.0	10.0	2.0
Grass	Varies	Varies	Varies

ACKNOWLEDGMENTS

This work was supported by the FHWA, U.S. Department of Transportation, and the U.S. Department of Agriculture Forest Service. State highway agencies of Arizona, Arkansas, Missouri, and Wyoming, and the U.S. Geological Survey assisted in gathering field data. The writers wish to express their appreciation to J. Sterling Jones for his valuable comments and

suggestions. They also acknowledge the assistance of Mike Mussetter in handling embankment construction and data collection and that of George K. Cotton and Rebecca Summer in literature search and review.

REFERENCES

1. Simons, Li and Associates, Inc. *Presentation of Field Data on Embankment Damage Due to Flood Overtopping*. Progress Report for Task A. FHWA, U.S. Department of Transportation, Jan. 1984.
2. H. W. Hjalmarson. *Flood Characteristics and Highway Damage at Five Arizona Sites, Flood of October 1983*. U.S. Geological Survey; FHWA, U.S. Department of Transportation, Tucson, Ariz., Sept. 1984.
3. C. E. Kindsvater. Discharge Characteristics of Embankment-Shaped Weirs. USGS Water-Supply Paper 1617-A. *Studies of Flow of Water Over Weirs and Dams*, U.S. Geological Survey, 1964.
4. J. N. Bradley. *Hydraulics of Bridge Waterways*. Hydraulic Design Series 1. FHWA, U.S. Department of Transportation, 1973.
5. J. Gessler. Beginning and Ceasing of Sediment Motion. In *River Mechanics*, edited and published by H. W. Shen, Fort Collins, Colo., 1971, Chapter 7.
6. E. T. Smerdon and R. P. Beasley. Relation of Compaction and Other Soil Properties to Erosion Resistance of Soils. *Transactions*, ASCE, Vol. 8, 1959.
7. E. T. Smerdon and R. P. Beasley. *The Tractive Force Theory Applied to Stability of Open Channels in Cohesive Soils*. Research Bulletin 715. Agricultural Experiment Station, College of Agriculture, University of Missouri, Columbia, Oct. 1959.
8. J. C. McWhorter, T. G. Carpenter, and R. N. Clark. *Erosion Control Criteria for Drainage Channels*. Mississippi State Highway Department, Jackson; FHWA, U.S. Department of Transportation; Agricultural Experiment Station, Mississippi State University, State College, March 1968.
9. V. T. Chow. *Open-Channel Hydraulics*. McGraw-Hill Book Company, New York, 1959.
10. R. Ariathurai and K. Arulanandan. Erosion Rates of Cohesive Soils. *Journal of the Hydraulics Division*, ASCE, Vol. 104, No. HY2, Feb. 1978, pp. 279–283.
11. S. P. Chee. Design of Erodible Dams. *Proc., International Conference of Water Resources Engineering*, Asian Institute of Technology, Bangkok, Thailand, Vol. 1, 1978, pp. 105–113.
12. V. R. Schneider and K. V. Wilson. *Hydraulic Design of Bridges with Risk Analysis*. Report FHWA-TS-80-226, FHWA HDV-21. U.S. Geological Survey; Office of Development, FHWA, U.S. Department of Transportation, March 1980.
13. Y. H. Chen and G. K. Cotton. *Design of Roadside Channels with Flexible Linings*. Hydraulic Engineering Circular 15. FHWA, U.S. Department of Transportation, Feb. 1986.
14. Y. H. Chen and B. A. Anderson. *Development of a Methodology for Estimating Embankment Damage Due to Flood Overtopping*. Simons, Li & Associates, Inc., Fort Collins, Colo.; FHWA, U.S. Department of Transportation; U.S. Department of Agriculture Forest Service, March 1986.